# A Basic Concept of the Nonlinear Oscillator-Based Hough Transform Implementation to Improve the Voting Procedure in the Scheme of Continuous Dual Spaces

**Amarbold Purev**
*Graduate School of Life Science and Systems Engineering, Kyushu Institute of Technology,*
*2-4 Hibikino, Wakamatsu, Kitakyushu 808-0196, Japan*

**Hiroaki Wagatsuma**
*Graduate School of Life Science and Systems Engineering, Kyushu Institute of Technology,*
*2-4 Hibikino, Wakamatsu, Kitakyushu 808-0196, Japan*
*Email: purev.amarbold118@mail.kyutech.jp, waga@brain.kyutech.ac.jp*

**Abstract**

Hough transform is a well-known algorithm to detect arbitrary lines in the image. The algorithm consists of two steps, mapping image edges to parameter space and voting to find a solution. The first step is executed in the continuous space, while the second relies on counting votes in discrete mesh, which increases susceptibility to noise. In the present study, we propose attractor dynamics in coupled nonlinear oscillators instead of discrete voting. In our computer experiment, image pixels were mapped to the parameter spaces and attracted to the crossing point of lines in the space. This approach may contribute to line detections in the image and other shape detections using a consistent mathematical formulation.

*Keywords*: Hough transform, line detection, nonlinear dynamics, coupled nonlinear oscillators, Kuramoto model

## 1. Introduction

The line detection from image data has the greatest need in computer vision [1][2][3], as the primitive component to form objects in the image [4]. The Hough Transform (HT) is the most frequent method to solve the problem, and the idea of the method is mathematically reasonable for the detection to project multiple line elements to the parametric space for generating a unique concentrating point. The projection of image data is treated between continuous spaces as Cartesian and polar coordinate systems; however, the finding of the concentration point is executed in a voting procedure in the discrete grids. In the comparison with the former process, the latter voting procedure causes a trade-off problem as the resolution-dependent noise removal effect. Apparently, high-resolution grids require a high computational cost. In the drawback of the method, another solution is expected to replace the latter procedure by using a mathematical treatment in the continuous space dynamics. Interestingly, convergence dynamics is known in the nonlinear dynamics, especially in attractor dynamics. According to the description of ordinary differential equations, those dynamics can be reconstructed in the computer experiment based on the numerical integration method, for instance, Euler method and Runge-Kutta method. If the dual space projection in HT and a natural convergence of moving points to represent a single line based on the nonlinear dynamics can be integrated, it provides a new method to solve the drawback of the original HT.

In the present paper, we focused on the mathematical solution of the straight-line detection, which can be derived from nonlinear oscillator dynamics providing synchronization phenomena in a limit cycle as well as the projection space of HT. If it is possible, moving points are concentrating automatically to detect the crossing points of lines in the projection space. Thus, the voting procedure is no longer necessary. In the section 2, the projection mechanism from Cartesian coordinate system to the polar coordinate system and its algorithm for computer experiments were reviewed, and a representative nonlinear oscillator dynamic was introduced for the replacement of the voting procedure in the section 3. In the section 4, the proposed system was formulated as the noise-robust line detection method, followed by results of the computer experiments in the section 5 and conclusion in the section 6.

## 2. Hough Transform Method

The Hough Transform (HT) is a method used in image analysis to detect shapes in an image [5]. The technique was introduced by Paul Hough in 1962 and has since been used in a variety of applications [6][7][8]. HT works by transforming the coordinates of edge points in an image from Cartesian coordinates to a more compact representation in parameter space [9].

$$\rho = x\cos(\theta) + y\sin(\theta) \quad (1)$$

Eq. (1) takes the coordinates of points in $XY$ plane and projects into parameter space. Thus, every point in $XY$ plane becomes a sine wave. Intersection of these sine waves give length value $\rho$, angle value $\theta$, which is a line perpendicular to the line through edge points. This transformation is shown in Figure 1.

To find intersection of edge points in Figure 1(b) HT method creates an accumulation array with $R \times T$ size consisting of zero values. $R$ is the number of rows for the $\rho$ value, and $T$ is the number of columns for $\theta$ value. For each value $\theta$, the $\rho$ value for each point is calculated, and the closest $\rho$ value in the accumulation array is incremented by 1. This process is called the voting procedure of HT. After passing through all columns of the accumulation array, the cell with the highest point determines the characteristics of the perpendicular line. This transformation allows for the detection of shapes to be reduced to a peak detection problem in parameter space.

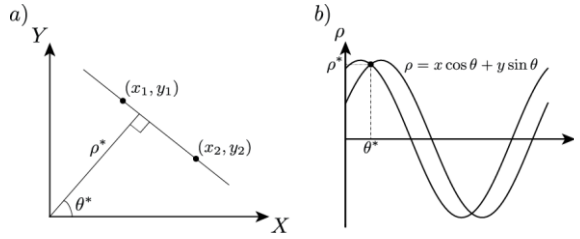


Fig. 1 Hough transformation. a) Representation of points $(\boldsymbol{x_1}, \boldsymbol{y_1})$ and $(\boldsymbol{x_2}, \boldsymbol{y_2})$, a line perpendicular to them with length $\boldsymbol{\rho}^*$ and angle $\boldsymbol{\theta}^*$ in image space. b) Transformed points as sine waves in parameter space.

One of the key advantages of the HT method is its simplicity, which allows for parallel processing of information. This makes the method robust to noise and allows for the detection of partially occluded or deformed shapes. Additionally, the method can be configured to detect a specific number of shapes in an image.

However, the simplicity of the HT method becomes a disadvantage when trying to detect shapes other than straight lines. The number of calculations increases as the number of parameters needed to describe the shape increases [10][11]. For example, detecting a circle in an image would require a three-dimensional accumulation array for the center coordinates of the circle $(x, y)$ and its radius $r$. Researchers have attempted to improve the efficiency of the HT method through software implementations [12][13][14][15], hardware acceleration [16], and the use of neural networks [17].

The use of an accumulation array in HT also presents challenges, as the size of the array needs to be fine-tuned for accurate detection. If the array is too small, the method loses accuracy, and if it is too large, the computation becomes expensive. Algorithm 1 describes the computer program algorithm for traditional HT.

**Algorithm 1. Classic HT for Line Detection**

**Data:** $(x, y)$ locations of edges in image space
**Result:** $(\rho, \theta)$ values of a cell with maximum vote
*Initialization.* Given number of rows $R$ for $\rho$ and number of columns $T$ for $\theta$, create accumulation array with zero values for $N$ number of edges in the image space.

**for** $i = 1$ to $i_N$ **do**
  **for** $t = 1$ to $T$ **do**
    calculate $\rho_i = x_i\cos(\theta) + y_i\sin(\theta)$
    find closest $R$ row to $\rho_i$
    increment cell value by 1 with location $(R, t)$
  **endfor**
**endfor**

As shown in Algorithm 1, HT only detects lines that are infinite in length. This is because the HT represents lines using their parameters, which do not include information about the length of the line. Thus, the HT cannot detect lines of finite length.

## 3. Nonlinear Oscillator Dynamics

### 3.1. *Kuramoto model*

The Kuramoto model (KM) is a mathematical model used to study synchronization in oscillators [18]. It is commonly used in fields such as physics [19][20], biology [21], and chemistry, and has been applied in various contexts, including neurophysiology [22][23], distributed power generation [24][25], and secure communication [26][27]. In this paper, we propose to use the modified model of KM to classify edges in digital images based on their collinearity.

The general form of the KM is defined by the following equation

$$\dot{\varphi}_i = \omega_i + \frac{K}{N}\sum_{j=1}^{N}\sin(\theta_j - \theta_i). \quad (2)$$

Eq. (2) describes a system of $N$ limit-cycle oscillators with natural frequencies $\omega_i$, phases $\theta$, and coupling constant $K$. The coupling between oscillators is based on the sine of their phase differences, and the time variation of phases follows first-order dynamics.

The use of the KM in image processing is rare because oscillators are dynamic objects, whereas edges in images are static. However, researchers in [28] have used it in color image segmentation, where they generated three oscillating curves corresponding to the pixel values of red, green, and blue for color images by a coupled network to produce superposition of oscillation for image pixels.

Nevertheless, we propose to use the attractor dynamics of coupled nonlinear oscillators in the KM to transform edge locations from discrete to continuous space. This allows for the classification of edges in parameter space using the KM, that will eliminate the need for an accumulation array in the HT method.

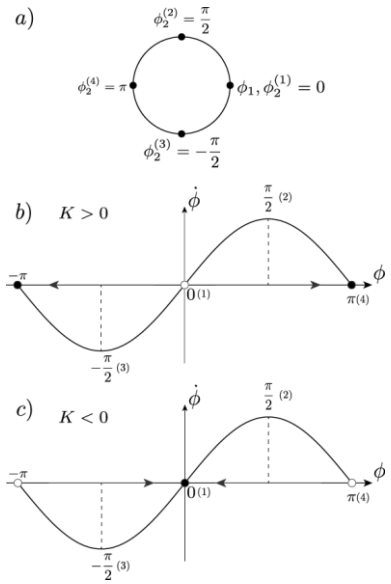


Fig. 2 Interaction between two nonlinear oscillators $\boldsymbol{\varphi_1}$and $\boldsymbol{\varphi_2}$. a) Initial positions. Behavior of the second oscillator b) $\boldsymbol{K > 0}$ c) $\boldsymbol{K < 0}$. Black dot represents stable point, white dot represents unstable point.

In order to understand how the KM can be used to detect lines in images, it is necessary to first analyze the behavior of simple systems. By studying their behavior, it will be possible to develop a model that can accurately classify edges in images based on their collinearity.

### 3.2. *Stability Analysis of two coupled Kuramoto oscillators*

Suppose that a system with two oscillators, $\dot{\varphi}_1$ and $\dot{\varphi}_2$, is given and behaves according to

$$\begin{cases}\dot{\varphi}_1 = 0\\ \dot{\varphi}_2 = K\sin(\varphi_2 - \varphi_1)\end{cases} \quad (3)$$

and subject to initial conditions $\varphi_i(0) = \varphi_i^0$, where $\varphi$ is the phase of the $i$th oscillator, $K$ is the coupling strength.

For simplification, we assumed $\dot{\varphi}_1 = 0$ in all cases, while concentrating on the dynamics of the second oscillator with initial values $\varphi_2^{(n)} = [0, \pi/2, -\pi/2, \pi], n = 1 \ldots 4$, as shown in Figure 2.

We now give the definition of phase synchronization.

**Definition 1.** Let $\{\boldsymbol{\varphi_i(t)}\}_{\boldsymbol{i=1}}^{\boldsymbol{2}}$ be solution of our system. We say the oscillators converge to phase synchronization if

$$\lim_{t\to\infty}\left|\varphi_i(t) - \varphi_j(t)\right| = 0, \quad \text{for } i \neq j. \quad (4)$$

Let's see the behavior of our system given by Eq. (3) with different initial conditions

**Example 1.** $\varphi_1(0), \varphi_2(0) = 0$

It is easy to see that the corresponding solution is $\varphi_1(t) = 0$ and $\varphi_2(t) = 0$. Hence there is phase synchronization.

**Example 2.** $\varphi_1(0) = 0, \varphi_2(0) = \frac{\pi}{2}, K > 0$

$$\begin{aligned}\varphi_2(t) &= K\sin\left(\frac{\pi}{2} - 0\right)\\ &= K\sin\left(\frac{\pi}{2}\right)\\ &= K\end{aligned} \quad (5)$$

Since $K > 0, \dot{\varphi}_2(t) \to \pi$ the second oscillator converges to the anti-phase.

**Example 3.** $\varphi_1(0) = 0, \varphi_2(0) = -\frac{\pi}{2}, K > 0$

$$\begin{aligned}\varphi_2(t) &= K\sin\left(-\frac{\pi}{2} - 0\right)\\ &= K\sin\left(-\frac{\pi}{2}\right)\\ &= -K.\end{aligned} \quad (6)$$

Since $\dot{\varphi}_2(t) < 0, \dot{\varphi}_1(t) \to -\pi$ the second oscillator converges to the anti-phase as well.

**Example 4.** $\varphi_1(0) = 0, \varphi_2(0) = \pi, K > 0$

$$\begin{aligned} \varphi_2(t) &= K\sin(\pi - 0) \\ &= K\sin(\pi) \\ &= 0 \end{aligned} \tag{7}$$

With the initial position for $\varphi_2(0) = \pi$ and $\varphi_2(t) = 0$, the second oscillator started at the anti-phase stable point of $\pi$ and do not move as $t \to \infty$.

Even though two oscillators do converge in Example 1, the 0 point is unstable as shown in Examples 2-4. Therefore, the system given by Eq. (3) converges to anti-phase. However, if the coupling strength has negative value, after doing same calculations as the above examples, we can see that the two oscillators do converge.

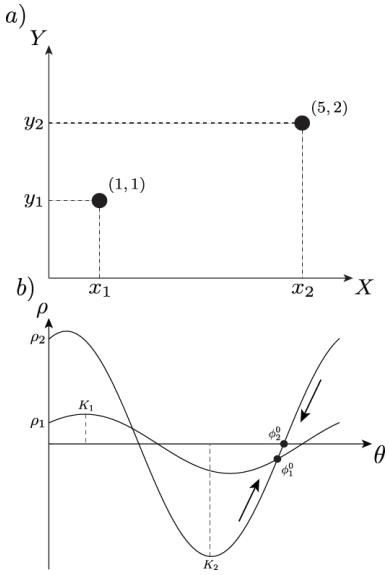


Fig. 3 Example of points (1,1) and (5,2). a) Image space. b) Hough space.

## 4. Proposed System for Noise-Robust Line Detection

### 4.1. *Hough Transform line detection for two points using coupled nonlinear oscillators*

The traditional HT method is described in Section 1.1 Instead of the traditional HT voting scheme, we propose replacing it with a nonlinear system of equations. Each point in the image space is treated as an individual nonlinear oscillator and coupled together with the following system of equations

$$\begin{cases} \dot{\varphi}_1 = 0 \\ \dot{\varphi}_2 = \dfrac{\rho_1 - \rho_2}{K^2} + (\varphi_1 - \varphi_2) \end{cases} \tag{8}$$

and subject to initial conditions $\varphi_i(0) = \varphi_i^0$, where $\varphi$ is the phase of the $i$th oscillator, $\rho$ is the Hough amplitude at the $\varphi$ phase and $K$ is the coupling strength based on the maximum amplitude of the $\rho$ value.

To find the intersection of two points in the Hough space, $\rho$ and $\theta$ values of each oscillator should converge. Similar to Eq. (3), we will set $\dot{\varphi}_1 = 0$ and concentrate on converging the second point to the first one. Which means, the oscillator $\dot{\varphi}_1$ will attract $\dot{\varphi}_2$ to itself.

Therefore, setting the initial phase of the first oscillator is crucial and we find its location analytically, where two sinusoidal lines intersect, which we can derive from the following assumption

$$\begin{aligned} \rho_1 &= \rho_2 \\ x_1\cos\theta + y_1\sin\theta &= x_2\cos\theta + y_2\sin\theta \\ \theta &= \tan^{-1}(-(x_1 - x_2)/(y_1 - y_2)). \end{aligned} \tag{9}$$

Accordingly, we set the initial phase of the first oscillator to $\varphi_1^0 = \tan^{-1}(-(x_1 - x_2)/(y_1 - y_2))$. For the initial phase of the second point, we are setting it at the fixed point of the Hough line, which means $\rho_2 = 0$, and with the same calculation as Eq. (9) the $\theta = \tan^{-1}(-x_2/y_2)$, and the starting position of the second oscillator $\varphi_2^0 = \tan^{-1}(-x_2/y_2)$. Coupling strength $K$ is the maximum of the $\rho$ value for each Hough line and equals to $K_i = x_i^2 + y_i^2$.

However, to avoid the anti-phase synchronization situation same as in Section 2.1 the sign changing rule must be applied.

Example 5 shows the verification of the above method.

**Example 5.** Two points, $p_1 = (x_1, y_1) = (1,1)$ and $p_2 = (x_2, y_2) = (5,2)$ are given in the image space, as shown in Figure 3. Initial values should be calculated to synchronize two oscillators for the coupling the same as Eq. (9). $\varphi_1^0 = \tan^{-1}(-(x_1 - x_2)/(y_1 - y_2)) = 4.9574$ rad, $\varphi_2^0 = \tan^{-1}(-x_2/y_2) = 5.0929$ rad, $K_2 = x_2^2 + y_2^2 = 29$.

From Figure 3, it is clear that $\varphi_i^0$ has 2 roots for each oscillator in $2\pi$ period. Therefore, depending on the location of the initial phase of the oscillator our proposed model should have the ability to change the sign. To first determine which direction the oscillator should move, the slope of the second Hough line should be calculated by the first derivative of $\rho$ function

$$\frac{d\rho}{d\theta} = y\cos\theta - x\cos\theta. \tag{10}$$

In total there are four different cases are possible

(i) $\varphi_1^0 > \varphi_2^0,\ \rho_2'(\varphi_2^0) > 0$
(ii) $\varphi_1^0 < \varphi_2^0,\ \rho_2'(\varphi_2^0) < 0$
(iii) $\varphi_1^0 > \varphi_2^0,\ \rho_2'(\varphi_2^0) < 0$
(iv) $\varphi_1^0 < \varphi_2^0,\ \rho_2'(\varphi_2^0) > 0$

After analyzing the possibilities, the four different possibilities can be classified into two groups (i, ii) and (iii, iv), which results in the same behavior. Then Eq. (8) transforms into the following system of equations

$$\begin{cases} \dot{\varphi}_1 = 0 \\ \dot{\varphi}_2 = \dfrac{\rho_1 - \rho_2}{K^2} + (\varphi_1 - \varphi_2), & \text{if A or B} \\ \dot{\varphi}_2 = \dfrac{\rho_2 - \rho_1}{K^2} + (\varphi_1 - \varphi_2), & \text{if C or D} \end{cases} \tag{11}$$

where $A = (\varphi_1^0 > \varphi_2^0, \varphi_2'(\varphi_2^0) < 0)$ , $B = (\varphi_1^0 < \varphi_2^0, \rho_2'(\varphi_2^0) > 0)$ , $C = (\varphi_1^0 > \varphi_2^0, \rho_2'(\varphi_2^0) > 0)$ , $D = (\varphi_1^0 < \varphi_2^0, \rho_2'(\varphi_2^0) < 0)$.

The Eq. (11) is simulated by using the Algorithm 2 below. We used Runge-Kutta 4th order method (RK4) to calculate first order derivative in our computer simulation.

**Algorithm 2. Classic HT for Line Detection**

**Data:** $(x, y)$ locations of $i = 1, \dots, N$ edges in image space
**Result:** $(\rho, \theta)$ values that represent a line
*Initialization. Calculate* $\varphi_i^0,\ i = 1, \dots, N$
**for** $iter = 1$ to $maxL$ **do**
  **for** $rk = 1$ to 4 **do**
    **if** A or B **then**
      Calculate $\dot{\varphi}_i$ with + sign
    **else**
      Calculate $\dot{\varphi}_i$ with − sign
    **endif**
    RK4 approximation
  **endfor**
**endfor**

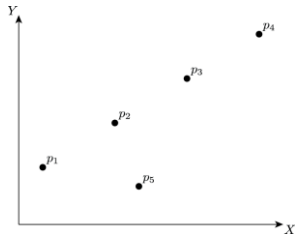


Fig. 4 Image space of five points

## 5. Results of Computer Experiments

In this section, we present the results of our proposed algorithm on multiple setups and provide an evaluation of correct detection as well as error.

Example 6 shows how the oscillators converge if a noncollinear edge exists in the image.

**Example 6.** $N = 5,\ p_1 = (1,3),\ p_2 = (4,5.33),\ p_3 = (7,7.76),\ p_4 = (10,10),\ p_5 = (5,2)$

In Example 6, five points are given, and the first point is the attractor, as shown in Figure 4. In the first part of the example $p_1$ is the attractor. Since, $p_1$ is part of the line through $p_1$ and $p_4$, oscillators converge into two groups. However, if the attractor is the outlier, such as $p_5$, oscillators converge into four groups. Notice that oscillators converged along the attractor's Hough line (dashed line in Figure 5).

We have also tested our method in the synthetic image with noise in two different scenarios, the same line with different noise and a different line with the same noise. The image has 100 collinear points and 1000 noise points in both scenarios with 20 samples each.

Table 1 and Table 2 shows the ratio of detected line points and errors. The threshold $\varepsilon = [10^{-3}, 10^{-4}, 10^{-5}]$ has been used to determine ratios. The distance $D$ between $(\rho, \varphi)$ values should be less than the threshold $\varepsilon$ and was calculated by the following formula

$$D = \sqrt{\left(\varphi_i - \varphi_j\right)^2 + \left(\rho_i - \rho_j\right)^2} < \varepsilon, \tag{12}$$

where $\varphi$ is the phase, $\rho$ is the Hough value at the phase $\varphi$ for the $i$th and $j$th oscillators, respectively.

The detected line points or cover ratio equals

$$CR = \frac{|LP| - |\text{NofCover}|}{|LP|}, \tag{13}$$

where $LP = \{1,2, \dots, 100\}$ set of collinear points, $\text{NofCover} = |LP| - |DP|$ set difference of collinear points and all detected points.

The error ratio is calculated as follows

$$ER = \frac{|DP - LP|}{|pD|}, \tag{14}$$

where $pD$ is set of all points, including collinear and noise.

From Table 1 and Table 2 we can see that the highest cover ratio $CR$ and lowest error ratio $ER$ occurs, when $\varepsilon < 10^{-4}$ at the iteration 125. Note that if the accuracy requirement increases, the time it takes to converge also increases ($\varepsilon = 10^{-5}, iter = 500$).

Figure 6 shows the convergence process in the parameter space for Table 1. Furthermore, Figure 7 shows the example of detected points in parameter and image spaces, respectively.

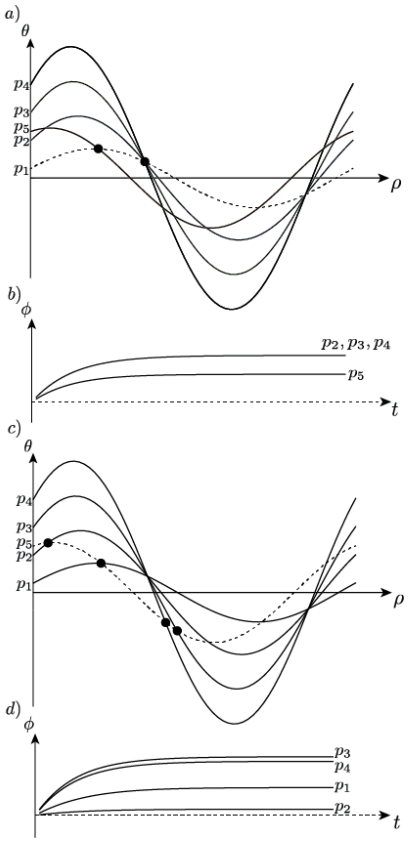


Fig. 5 Convergence of points with different attractors $\boldsymbol{p_1}$ – (a, b) and $\boldsymbol{p_5}$ – (c, d).

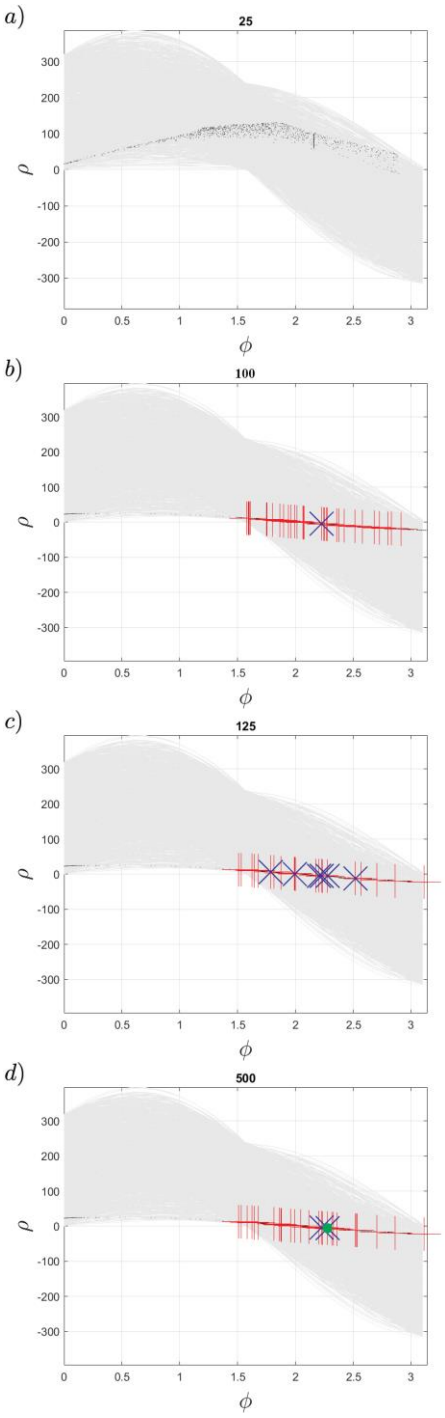


Fig. 6 A convergence process of moving points on projected lines in a) 25, b) 100, c) 125, d) 500 iteration periods. Colored marks represent $(\boldsymbol{\rho}, \boldsymbol{\theta})$ convergence points, when threshold value $\boldsymbol{\varepsilon = 10^{-3}}$(red "+"), $\boldsymbol{10^{-4}}$ (blue "X"), $\boldsymbol{10^{-5}}$ (green "dot").

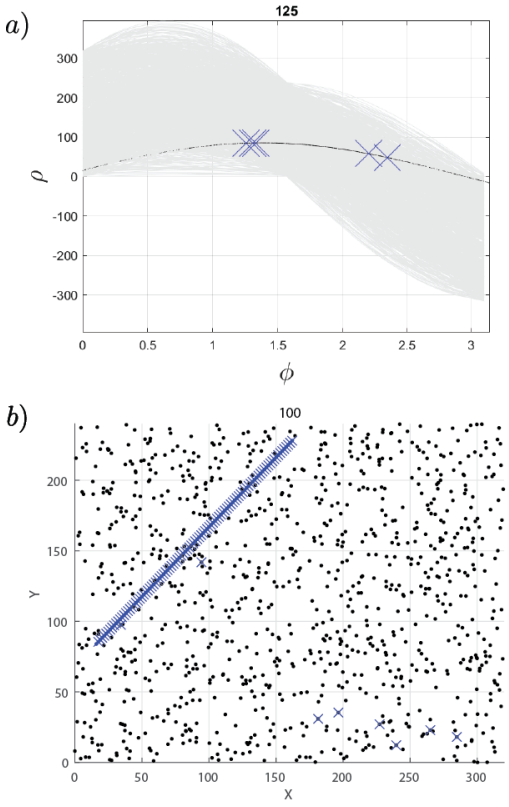


Fig. 7 Example of detected collinear points for same line different noise with $\boldsymbol{\varepsilon = 10^{-4}}$ and $\boldsymbol{iteration = 125}$. a) clustered points in parameter space b) detected points in image space (detected points are plotted with blue "X" sign)

## 6. Conclusion

Our method demonstrated the elimination of the use of the voting scheme of the classic HT by using coupled nonlinear oscillator dynamics.

The advantage of this method is that the user does not need to have any experience using the method since creating a specific-sized accumulation array is unnecessary. However, this method selects one point at a time, checks for colinear points, and clusters them into groups, which will have a slower implementation than the classic HT.

Further improvement of the method will improve HT's infinite line problem by clustering points into groups yielding finite lines.

## Acknowledgements

This work was supported in part by JSPS KAKENHI (16H01616, 17H06383), Project on Regional Revitalization Through Advanced Robotics (Kyushu Institute of Technology/Kitakyushu city, Japan) and the New Energy and Industrial Technology Development Organization (NEDO).

Table 1. Average ratio of detected line points and errors for different line same noise at iterations (%).

| $\varepsilon$ | 25 | | 50 | | 75 | | 100 | | 125 | | 500 | |
|---|---|---|---|---|---|---|---|---|---|---|---|---|
| | CR | ER | CR | ER | CR | ER | CR | ER | CR | ER | CR | ER |
| $10^{-3}$ | 0 | 0 | 0 | 0.09 | 5.20 | 1.07 | **99.0** | **3.02** | 99.00 | 3.70 | 99.00 | 3.72 |
| $\mathbf{10^{-4}}$ | 0 | 0 | 0 | 0 | 0 | 0.01 | 4.95 | 0.11 | **99.00** | **0.34** | 99.00 | 0.45 |
| $10^{-5}$ | 0 | 0 | 0 | 0 | 0 | 0 | 0 | 0 | 19.80 | 0.02 | **99.00** | **0.05** |

Table 2. Average ratio of detected line points and errors for same line different noise at iterations (%).

| $\varepsilon$ | 25 | | 50 | | 75 | | 100 | | 125 | | 500 | |
|---|---|---|---|---|---|---|---|---|---|---|---|---|
| | CR | ER | CR | ER | CR | ER | CR | ER | CR | ER | CR | ER |
| $10^{-3}$ | 0 | 0 | 0.05 | 0.02 | 0.35 | 0.68 | **99.00** | **3.43** | 99.00 | 6.12 | 99.00 | 6.18 |
| $\mathbf{10^{-4}}$ | 0 | 0 | 0.05 | 0 | 0 | 0 | 0.10 | 0.04 | **99.00** | **0.52** | 99.00 | 0.61 |
| $10^{-5}$ | 0 | 0 | 0 | 0 | 0 | 0 | 0 | 0 | 0.05 | 0.02 | **99.00** | **0.04** |

## References


1. B. K. P. Horn, “Robot Vision”, MIT Press, 1986.
2. W. Chen, W. Wang, K. Wang, Z. Li, H. Li, S. Liu, “Lane departure warning systems and lane line detection methods based on image processing and semantic segmentation: A review”, JTTE (English Edition), Vol. 7, No. 6, pp. 748-774, 2020.
3. Q. Luo, X. Fang, L. Liu, C. Yang, Y. Sun, “Automated Visual Defect Detection for Flat Steel Surface: A Survey”, IEEE Transactions on Instrumentation and Measurement, Vol. 69, No. 3, pp. 626-644, 2020.
4. Q. -R. Wei, D. -Z. Feng, W. Zeng, J. -B Zheng, “Rapid line-extraction method for SAR images based on edge-field features”, IEEE Geoscience and Remote Sensing Letters”, Vol. 14, No. 10, pp. 1865-1869, 2017.
5. P. V. C. Hough, “Method and means for recognizing patterns”, US Patent 3069654A, 1962.
6. T. K. Greeshma, S. Priya, C. Chaithanya, “A Survey on Line Detection Techniques using Different Types of Digital Images”, IJARCET, Vol. 8, No. 5, pp. 162-168, 2019.
7. F. Tschopp, C. von Einem, A. Cramariuc, D. Hug, A. W. Palmer, R. Siegwart, M. Chli, J. Nieto, “Hough$^2$Map – Iterative Event-Based Hough Transform for High-Speed Railway Mapping”, IEEE Robotics and Automation Letters, Vol. 6, No. 2, pp. 2745-2752, 2021.
8. C. Dalitz, T. Schramke, M. Jeltsch, “Iterative Hough Transform for Line Detection in 3D Point Clouds”, Image Processing On Line, Vol. 7, pp. 184-196, 2017.
9. R. O. Duda, P. E. Hart, “Use of the Hough Transformation to Detect Lines and Curves in Pictures”, Communications of the ACM, Vol. 15, No. 1, pp. 11-15, 1972.
10. D. H. Ballard, “Generalizing the Hough transform to detect arbitrary shapes, Pattern Recognition, Vol. 13, No. 2, pp. 111-122, 1981.
11. N. Kiryati, Y. Eldar, A. M. Bruckstein, “A Probabilistic Hough Transform”, Pattern Recognition, Vol. 24, No. 4, pp. 303-316, 1991.
12. L. A. F. Fernandes, M. M. Oliveira, “Real-time line detection through an improved Hough Transform voting scheme”, Pattern Recognition, Vol. 41, No. 1, pp. 299-314, 2008.
13. H. F. Li, D. Pao, R. Jayakumar, “Improvements and Systolic Implementation of the Hough Transformation for straight line detection”, Pattern Recognition, Vol. 22, No.6, pp. 697-706, 1989.
14. S. Du, B. J. van Wyk, C. Tu, X. Zhang, “An improved Hough transform neighborhood map for straight line segments”, IEEE Transactions on Image Processing, Vol. 19, No.3, pp. 573-585, 2010.
15. N. Aggarwal, W. C. Karl, “Line detection in images through regularized Hough transform”, IEEE Transactions on Image Processing, Vol. 15, No. 3, pp. 582-591, 2006.
16. E. Hajjouji, S. Mars, Z. Asrih, A. E. Mourabit, “A novel FPGA implementation of Hough Transform for straight lane detection”, JESTECH, Vol. 23, No. 2, pp. 274-280, 2020.
17. M. W. Spratling, “A neural implementation of the Hough transform and the advantages of explaining away”, Image and Vision Computing, Vol. 52, No. 1, pp. 15-24, 2016.
18. J. A. Acebron, L. L. Bonilla, C. J. P. Vicente, F. Ritort, R. Spigler, “The Kuramoto model: A simple paradigm for synchronization phenomena”, Reviews of Modern Physics, Vol. 77, No. 1, pp. 137-185, 2005.
19. M. Ignatov, M. Ziegler, M. Hansen, H. Kohlstedt, “Memristive stochastic plasticity enables mimicking of neural synchrony: Memristive circuit emulates an optical illusion”, Science Advances, Vol. 3, No. 10, pp. e1700849, 2017.
20. M. Ignatov, M. Hansen, M. Ziegler, H. Kohlstedt, “Synchronization of two memristively coupled van der Pol oscillators”, Applied Physics Letters, Vol. 108, No. 8, pp. 084105, 2016.
21. H. Mizuhara, Y. Yamaguchi, “Human cortical circuits for central executive function emerge by theta phase synchronization”, NeuroImage, Vol. 36, No. 1, pp. 232-244, 2007.
22. T. Cattai, S. Colonnese, M. C. Corsi, D. S. Bassett, G. Scarano, F. D. V. Fallani, “Phase/amplitude synchronization of brain signals during motor imagery BCI tasks”, arXiv:1912.02745 [q-bio.NC], 2019.
23. V. Rohr, R. Berner, E. L. Lameu, O. V. Popovych, S. Yanchuk, “Frequency cluster formation and slow oscillations in neural populations with plasticity”, PLoS ONE, Vol. 14, No. 11, pp. e0225094, 2019.
24. P. A. Arinushkin, T. E. Vadivasova, “Nonlinear damping effects in a simplified power grid model based on coupled Kuramoto-like oscillators with inertia”, Chaos, Solitons & Fractals, Vol. 152, No. 1, pp. 111343, 2021.
25. Y. Guo, D. Zhang, Z. Li, Q. Wang, D. Yu, “Overviews on the applications of the Kuramoto model in modern power system analysis, International Journal of Electrical Power & Energy Systems, Vol. 129, pp. 106804, 2021.
26. A. Argyris, D. Syvridis, L. Larger, V. A. Lodi, P. Colet, I. Fischer, J. G. Ojalvo, C. R. Mirasso, L. Pesquera, K. A. Shore, “Chaos-based communications at high bit rates using commercial fibre-optic links”, Nature, Vol. 438, No. 7066, pp. 343-346, 2005.
27. P. Feketa, A. Schaum, T. Meurer, D. Michaelis, K. Ochs, “Synchronization of nonlinearly coupled networks of Chua oscillators”, IFAC-PapersOnLine, Vol. 52, No. 16, pp. 628-633, 2019.
28. X. Lu, Y. Qiao, X. Chen, J. Miao, L. Duan, “Color Image Segmentation Based on Modified Kuramoto Model”, Procedia Computer Science, Vol. 88, No. 1, pp. 245-258, 2016.

## Authors Introduction

Mr. Amarbold Purev

He received his Master's degree from the School of Mechanical Engineering and Transportation, Mongolian University of Science and Technology, Mongolia in 2019. He is currently a Doctoral course student in Kyushu Institute of Technology, Japan.

Dr. Hiroaki Wagatsuma

He received his M.S., and Ph.D. degrees from Tokyo Denki University, Japan, in 1997 and 2005, respectively. In 2009, he joined Kyushu Institute of Technology, where he is currently Professor of the Department of Human Intelligence Systems. His research interests include nonlinear dynamics and robotics. He is a member of IEEE.